MECSOL 2019 - Proceedings of the 7th International Symposium on Solid Mechanics,
G. C. P. Martins, C. F. Bandeira, G. Wegmann, J. T. P. de Castro, ABCM, Sao Carlos, SP, Brazil, April 15th to 17th, 2019

Evaluation of the Fatigue Limits of Aluminum Alloys by Thermographic and εN techniques

Gabriela Cristina Paiva Martins, Carlos Filipe Cardoso Bandeira, Gabriela Wegmann Lima, Jaime Tupiassú Pinho de Castro

Mechanical Engineering Department, Pontifical Catholic University of Rio de Janeiro (PUC-Rio), Rua Marquês de São Vicente 225, Rio de Janeiro, RJ 22453-900, Brazil;

Abstract: It is well-known that when a material is subjected to cyclic loading, its temperature increases. Since fatigue damage is caused by cyclic plasticity, a dissipative process, such temperature increments are much more pronounced under loadings above the fatigue limit of the material. Based on this evidence, an efficient thermographic method was proposed as an alternative way to measure fatigue limits of steels. This work addresses the experimental problems associated with the evaluation of fatigue limits of aluminum alloys using a variation of the thermal approach proposed by La Rosa and Risitano, which correlates temperature increments with several loading amplitudes and defines the fatigue limit as the stress below which no significant heat generation is measured. However, unlike in steels, in aluminum alloys the number of cycles needed to achieve temperature stabilization is highly dependent on the stress amplitudes, an issue that must be properly addressed in the measurement procedures. To verify the results obtained by thermography, the fatigue limit of the tested Al alloy (assumed to be associated, as usual to a life of $5{\cdot}10^8$ cycles) is estimated by extrapolating its εN curve measured by standard procedures to such very long life.

Keywords: Fatigue, Fatigue Limit, Thermographic Method, εN extrapolation.

INTRODUCTION

Fatigue is the mechanical failure mechanism that induces crack initiation and/or propagation under cyclic loads, in a gradual and stable process that can last up to the eventual fracture of the structural component. The fatigue or endurance limit S_L is defined as the stress amplitude below which the crack initiation process is not activated (at least at the surface of the components, since they may initiate as internal fish eye cracks under much longer gigacycle lives (Castro and Meggiolaro, 2016)). Even though S_L is a most important property for structural design purposes, its measurement by classical mechanical procedures is laborious and expensive. Indeed, both the Prot (1948) and the Dixon (1965) traditional methods require the test of many specimens (typically more than 10) during a very large number of cycles, to identify if they can last for lives longer than those associated with their fatigue limits. Such tests typically must last for at least 5 to 10 million cycles for steels, whereas for aluminum alloys they must last for much longer, usually $5{\cdot}10^8$ cycles or even more. Fast servohydraulic machines, working at say 60Hz, can apply about 5 million cycles per day. Hence, a single fatigue limit test for an Al alloy in such machines requires cycling one specimen for more than 3 months working around the clock, 24 h per day, 7 days per week, certainly a major practical problem. Even very fast rotating bending machines, working at say 10000 rpm, accumulate less than 15 million cycles per day. They consume much less energy than the servohydraulic machines, but do not solve the testing time problem. Only resonant ultrasonic testing machines working around 20kHz can perform such tests in reasonable times, but they are neither widely available nor versatile.

Hence, it is no surprise that most mechanical designs must rely on empirical estimations for fatigue limits. According to Castro and Meggiolaro (2016), fatigue limits S_L for steel and Al structural components e.g. can be estimated by Eq. (1) and (2), respectively. Such estimates depend on the ultimate strength S_U and on some empirical fatigue strength modifying factors, such as surface finish k_{sf}; component size k_{sz}, load type k_{lt} and notch sensitivity q (which are related to stress gradient effects near the critical point where the crack initiates), working temperature k_Θ; reliability k_{Rl}, fretting k_{ft}, etc.

$$\begin{cases} S_F(10^3) = k_\theta k_{Rl} \cdot 0.76 S_U, & S_U \le 1400MPa \\ S_F(10^3) = k_\theta k_{Rl} \cdot 0.67 S_U, & S_U > 1400MPa \\ S_L(10^6) = k_{sf} k_{sz} k_{lt} k_\theta k_{Rl} k_{ft} \cdot S_U/2, & S_U \le 1400MPa \\ S_L(10^6) = k_{sf} k_{sz} k_{lt} k_\theta k_{Rl} k_{ft} \cdot 700MPa, & S_U > 1400MPa \end{cases} \quad (1)$$

$$\begin{cases} S_F(10^3) = k_\theta k_{Rl} \cdot 0.82 S_U, & S_U \le 325MPa \\ S_L(5 \cdot 10^8) = k_{sf} k_{sz} k_{lt} k_\theta k_{Rl} k_{ft} \cdot 130MPa, & S_U > 325MPa \end{cases} \quad (2)$$

Even though purely elastic strains should cause no damage, some authors do not recognize fatigue limits for Al and for some other non-ferrous alloys, see Fig. 1.a. To avoid this problem for structural design purposes, their *SN* (Wöhler's) curves can be estimated by a two-step bi-parabolic approximation that leads to two straight lines in log-log plots, the second with a smaller slope starting at lives longer than a very long life N_L associated with a S_L-like stress. Haibach (1970) proposed Eq. (3) for steel components, and his idea can be adapted to describe the *SN* curves of non-ferrous components.

$$\begin{cases} NS_F^B = C, N \le N_L \\ NS_F^{2B-1} = C \cdot [S_L(N_L)]^{B-1},\ N > N_L \end{cases} \tag{3}$$

To avoid the need for testing too many specimens for a long time, La Rosa and Risitano (1999) proposed a robust procedure to measure fatigue limits by a remote sensing thermal technique using few specimens tested at much shorter times, which do not even need to be broken. They just correlate blocks of incremental stress amplitudes σ_a applied on standard fatigue specimens with the heat they generate on their surfaces due to the crack initiation process. The ratios of the maximum temperatures induced by the number of block cycles needed to stabilize them (after the so-called first thermal phase), $d\Theta_{max}/dN_1$, and the ratio of the applied stress amplitudes by the ultimate strength, σ_a/S_U, are used to evaluate the fatigue limit, as shown in Fig. 1.b.

In addition, to verify the fatigue limits measured by thermography, an extrapolation of *εN* data is used here. After obtaining the *εN* curve of the material by standard ASTM procedures, the alternated stress at $5 \cdot 10^8$ cycles, the life usually associated with fatigue limits of Al alloys, is calculated. Obviously, the ideal way of checking the values obtained by thermography would be to find the fatigue limit by standard Dixon or Prot procedures. However, the extrapolation of a properly measured *εN* curve is an alternative educated estimate that can be found in a much shorter time.

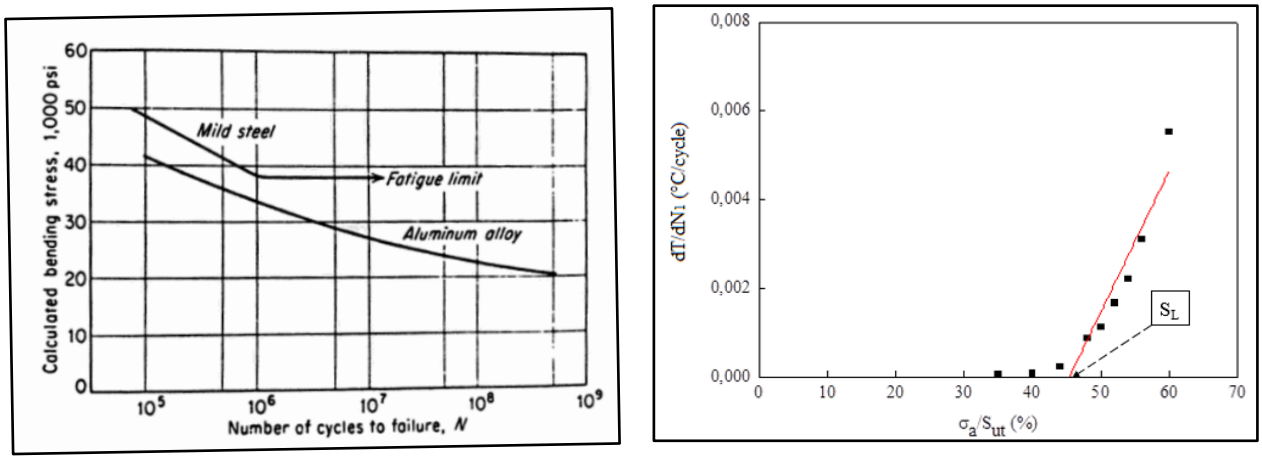

(a) (b)

Figure 1 – (a) Typical SN curve for mild steels and Al alloys, Boyer (1985); (b) S_L evaluation from thermal data

IR THERMOGRAPHY METHOD

La Rosa and Risitano proposed to map the temperature of the surface of fatigue specimens using a high-resolution infrared thermocamera. They say that when constant stress amplitude loading cycles above the fatigue limit are applied on steel specimens, their temperature increments increase during the first part of the test (phase 1), then remain almost constant for a while (phase 2), and finally suffer a rapid increase prior to failure (phase 3), as schematized in Fig. 2.

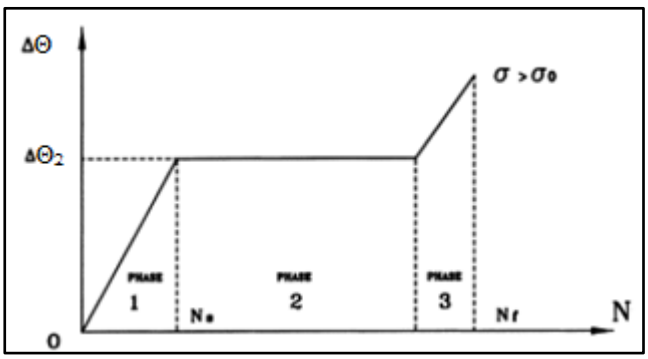

Figure 2 - Phases of the thermal behavior over the surface of a specimen

Based on the typical $\Delta\Theta \times N$ behavior of their steel fatigue specimens, La Rosa and Risitano proposed to determine fatigue limits by plotting temperature increments at the end of phase 1 ($\Delta\Theta_2$ in Fig. 2), or else temperature increase rates

$\partial\Theta/\partial N$ in phase 1 caused by different stress amplitude levels $\sigma_a = \Delta\sigma/2$ applied on a same specimen, which does not even need to be broken. They showed that such $\Delta\Theta \times \sigma_a$ or $\partial\Theta/\partial N \times \sigma_a$ curves typically have a bilinear trend with very different slopes $\partial\Delta\Theta/\partial\sigma_a$ or $\partial(\partial\Theta/\partial N)/\partial\sigma_a$, respectively, see Fig. 1.b again.

These two slopes can be used to recognize the transition from no fatigue damage below the fatigue limit to a damage accumulation process above it, and consequently the fatigue limit of the tested specimen. According to La Rosa and Risitano, operationally the fatigue limit S_L can be found by this thermographic method extending the straight line with highest slope until it across σ_a-axis. A variation of this technique will be used in this article.

εN EXTRAPOLATION METHOD

Traditional εN design procedures assume fatigue crack initiation is primarily caused by cyclic elastoplastic strain histories induced by service loads at the critical points of structural components. Such procedures can be used to estimate the fatigue crack initiation life from its measured Coffin-Manson curve, using its Ramberg-Osgood properties to correlate the stresses at critical points to theirs correspondent strain ranges. Such cyclic $\sigma\varepsilon$ curves are usually obtained by joining the tips of several concentric stabilized elastoplastic hysteresis loops, measured by testing several identical push-pull εN specimens at different fixed strain ranges $\Delta\varepsilon_i$, all with zero mean stresses and strains, as schematized in Fig. 3.a. The number of cycles needed to initiate a fatigue crack under a fixed strain range $\Delta\varepsilon$ is usually measured in push-pull εN tests identical to those used to measure hysteresis loops. So, the εN method assumes that strain ranges can be correlated with corresponding stress ranges by Ramberg-Osgood's equation, and with fatigue lives by Coffin-Manson's rule:

$$\varepsilon_a = \Delta\varepsilon/2 = \Delta\varepsilon_{el}/2 + \Delta\varepsilon_{pl}/2 = (\sigma_c/E)(2N)^b + \varepsilon_c(2N)^c \quad (4)$$

Countless tests confirm that fatigue crack initiation lives can indeed be well correlated with strain amplitudes $\varepsilon_a = \Delta\varepsilon/2$ imposed on fatigue specimens, as schematized in Fig. 3.b. Coffin-Manson's equation shows that elastic strains are negligible for very short lives, it tends to its plastic part in that so-called the low-cycle region, where $\Delta\varepsilon_{pl} >> \Delta\varepsilon_{el}$. Likewise, long lives are associate with almost purely elastic strain ranges, meaning $\Delta\varepsilon_{pl} << \Delta\varepsilon_{el}$, and this region of Coffin-Manson's curves tend to Wöhler's power function $NS^B = C$, where $B = -1/b$ and $C = (1/2)(\sigma_c)^{-1/b}$.

The extrapolation procedure to estimate the fatigue limit from Eq. (4) simply consists of first obtaining the εN curve for the Al alloy and then using its properties evaluate the stress range corresponding to a life of $N_L = 5{\cdot}10^8$ cycles. Since fatigue limits should in principle be associated with purely elastic loads, their stress values can be obtained from the corresponding strain ranges (for Al alloys ε_a(N = $5{\cdot}10^8$ cycles)) directly by Hooke's law, neglecting the plastic term contribution. Such estimates obviously improve with the number of long life tests included in the measured εN curve.

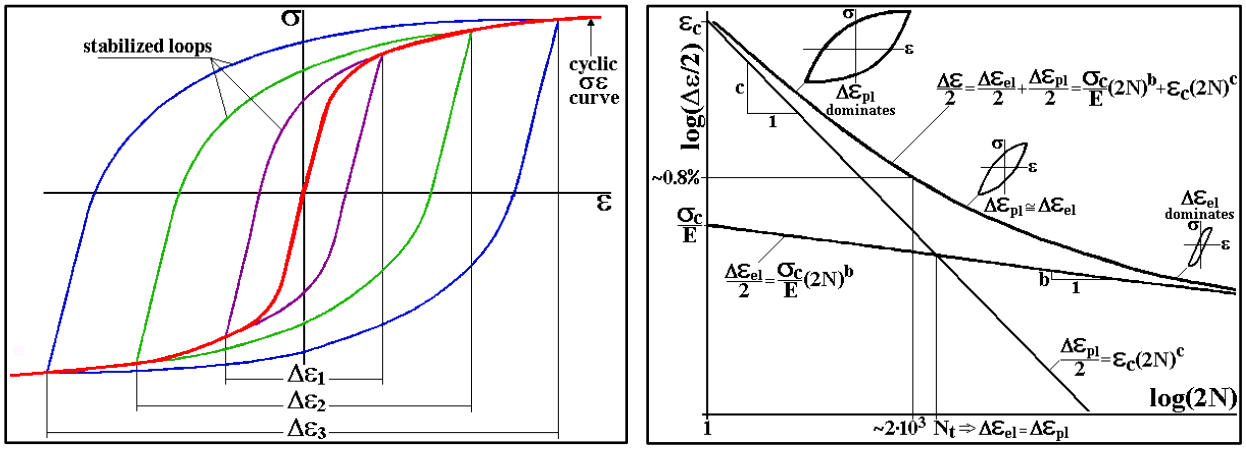

(a) (b)

Figure 3 – (a) Schematic concentric loops, and the cyclic σε curve obtained by joining their tips; (b) Scheme of the Coffin-Manson curve of a metallic alloy

MATERIAL AND EXPERIMENTAL PROCEDURES

The thermographic fatigue limit tests were made in a rotating bending machine under a load radio $R = -1$ at a frequency $f = 8500$ rpm. The hourglass-like fatigue specimens had a large constant radius and a polished surface (measured surface roughness $R_a = 0.099$ μm), see Fig 4.a. This is needed to minimize stress concentration effects and to ensure that their middle section is the critical one, see Fig. 4.b. Figure 4.c shows a specimen with its central part black-painted, to increase its emissivity and thus to improve the infrared camera performance. All specimens were dimensionally verified and stored in a humidity-controlled environment. Table 1 lists the chemical composition of the 6351-T6 Al alloy used in this article, whose basic tensile properties are yield strength $S_Y = 324$MPa and tensile strength $S_U = 352$MPa.

Table 1 – The Chemical Composition of the 6351-T6 Aluminum alloy

Mn	Si	Cr	Ni	Cu	Fe	Mg	Ti	Zn	Al
0.510	1.080	0.010	0.010	0.040	0.290	0.510	0.020	0.030	97.440

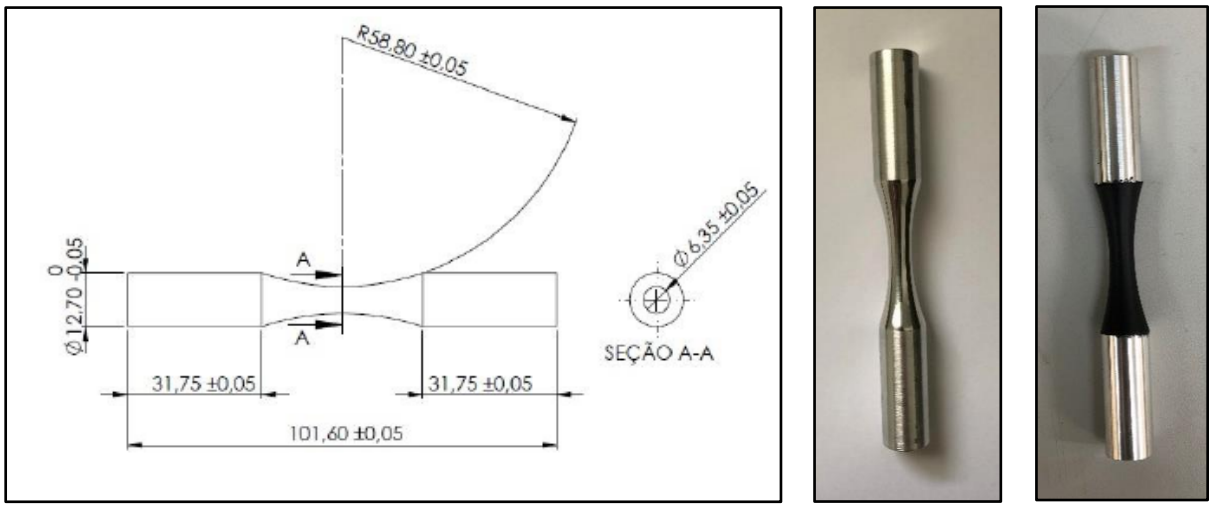

(a) (b) (c)

Figure 4 – Specimen: (a) geometry and dimensions; (b) as manufactured; (c) black painted

A compact, bench mounted rotating bending machine RBF 200 was used in all fatigue tests. Its major advantage is a high loading frequency, up to 10,000 rpm. The specimen surface temperature was continuously monitored by an infrared FLIR A320 camera with resolution of 320×240 pixels, data acquisition frequency 30Hz, and temperature sensibility 50mK. The temperature data was analyzed using the software ResearchIR from FLIR. In addition, a black cloth was used to cover the rotating bending machine and camera. Figure 5 shows the RBF 200 used in this article.

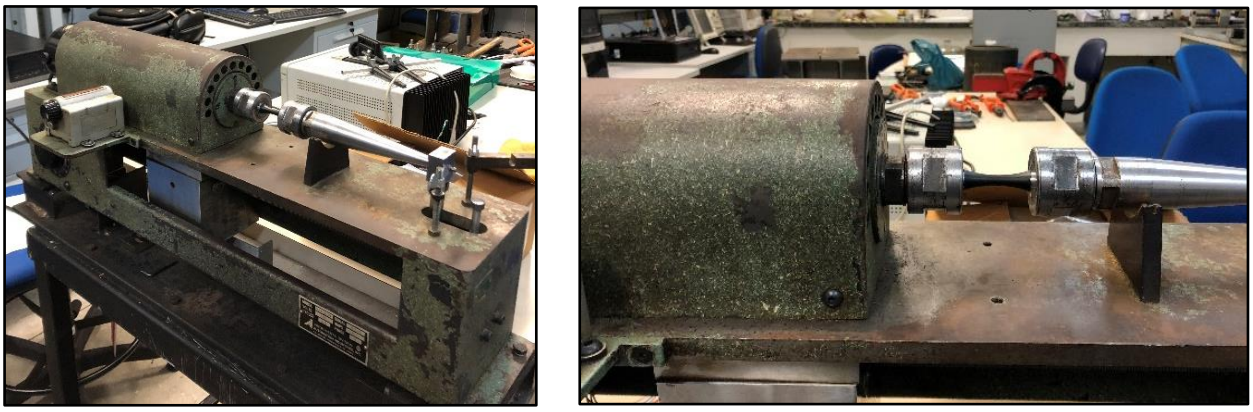

(a) (b)

Figure 5 - RBF 200: (a) overview; (b) lateral view

The εN curve was measured in standard fatigue tests conducted on a 100 kN Instron servo-controlled testing machine under a load radio $R = -1$ at a frequency $f = 2$ Hz, as illustrated in Fig. 6.a. All εN specimens were dimensionally verified, according to the ASTM E606 standard and proper care was taken to avoid delayed buckling of εN test specimens. Initially the loading train was aligned within ±0.01mm, to minimize load eccentricity effects. This step is most important to avoid parasitic bending moments during the εN tests. Notice in Fig. 6.c the very large radio of the εN specimens, to minimize stress concentration effects. Figure 6.d shows a polished 6351-T6 Al alloy specimen.

EXPERIMENTAL RESULTS

Figure 7.a shows a Θ_{max} versus number of cycles N plot for $\sigma_a/S_U = 0.7$. For this Al alloy, the variation of temperature is small and phase I is characterized by a small number of cycles compared of the specimen life; phase II includes most of the specimen life; and phase III is associated with a large temperature increase, where the specimen final fracture occurs in a much smaller number of cycles than N_1. Notice that the number of cycles N_1 depends on the amplitude of the stress, i.e. it varies significantly with the applied stress range. This is a characteristic of Al alloys, which do not have a cycle-independent thermal phase 1, as steel specimens do.

(a)

(b)

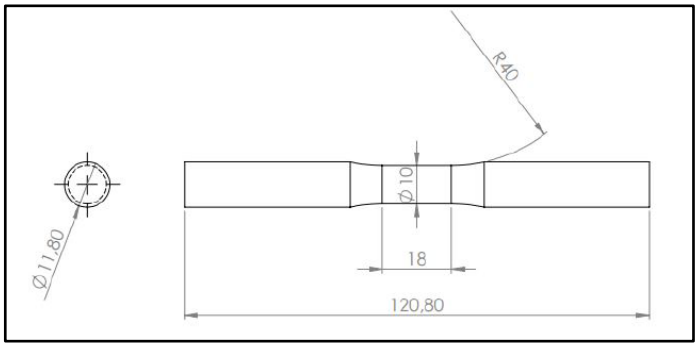

(c)

(d)

Figure 6 – (a) 100 kN Instron servo-controlled testing machine; (b) εN specimen with the controlling clip-gage mounted on it; (c) geometry and dimensions; (d) as manufactured

Other experimental results with different amplitudes of stress ($\sigma_a/S_U = 0.6$ and 0.8) were obtained and Tab. 2 lists the number of cycles and the variation of the surface temperature of the specimen in each phase. La Rosa and Risitano propose that the first phase of temperature increase is limited to a small number of cycles compared to the number of cycles needed to fail the specimen N_t. In general, not larger than 10% of the whole life of steel specimen for loads not close to the yield stress. However, the Al alloy tested in this work had a quite distinct behavior, because in each load amplitude its first thermal phase was a different fraction of the full life of the specimen. Their third phase, associated to the complete plasticization, shows a quick temperature increment, in a very small number of cycles.

Table 2 – Results from experimental tests with σ_a = 60%, 70% and 80% of S_U

Specimen	N_1 (cycle)	N_2 (cycle)	N_3 (cycle)	$\Delta\Theta_1$ (°C)	$\Delta\Theta_2$ (°C)	$\Delta\Theta_3$ (°C)
60% of S_U	78897	197540	15442	0.61	0.10	2.45
70% of S_U	49301	115158	9197	0.11	0.88	1.14
80% of S_U	16835	28674	3178	0.17	0.77	0.83

It is expected that the higher temperature is localized around the smaller section of the specimen where the failure occurs. It is interesting to note a larger rate $d\Theta/dN$ on the third thermal phase, due the rapid temperature increase which occurs because of the complete plasticization of a section of the specimen. Moreover, note that first phase of the thermal behavior of this material has a linear behavior, as shown in Fig. 7.a. In this way, it was possible to predict the number of cycles for each applied σ_a/S_U and the total time of the experimental test.

Moreover, one specimen was tested under increasing stress amplitude steps $\sigma_a/S_U = 0.2$, 0.3, 0.4, 0.5, 0.6, 0.7 and 0.8, each one lasting the number of cycles needed to characterize the first thermal phase, determined by fitting the line shown in Fig. 7.b. Figure 8.a shows the variation of the maximum temperature on the surface of the specimen along the number of cycles, from the smallest to the largest stress amplitude. It illustrates well that the more the stress amplitude increases, the more both the temperature increments $\Delta\Theta_1$ and its $d\Theta/dN_1$ rates increase with the amplitude of each load step and demonstrates the difficulty of analyzing the experimental data to determine the temperature variation $\Delta\Theta$ due to the lack of temperature stabilization of increasing stress amplitude graphs of the Al.

The next step will be to measure the temperature increase $d\Theta$ of each phase and it will be correlated with σ_a/S_U. In sequence, a linear regression is fitted to determine the value of S_L as the stress amplitude at intercept on the x-axis, e.g. Fig. 8.b. Therefore, it is concluded that the fatigue limit of this aluminum alloy is approximately 0.48 S_R, which corresponds to 168MPa.

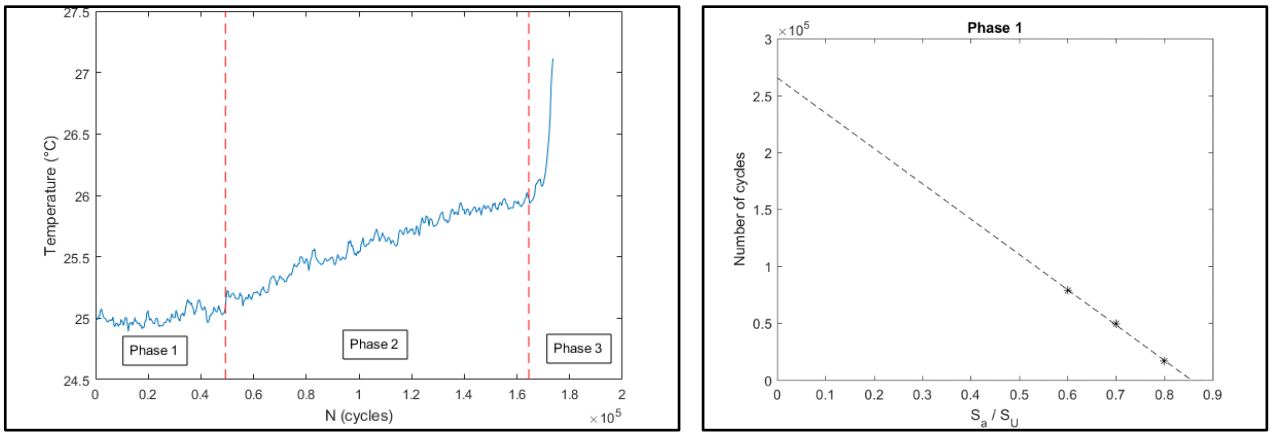

(a) (b)

Figure 7 – (a) Temperature versus cycles of 70% of S_U; (b) Adjustment of data from the first phase.

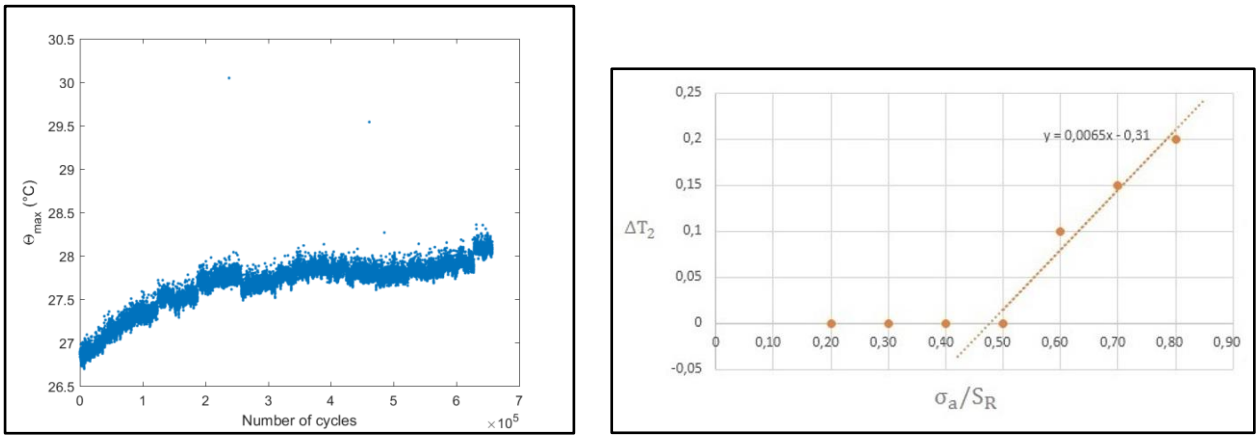

(a) (b)

Figure 8 – (a) T_{max} versus cycles under increasing load steps; (b) S_L evaluation from thermal data

For the εN tests, ten specimens were tested under a series of fixed strain ranges $\Delta\varepsilon = 0.4\%, 0.5\%, 0.6\%, 0.7\%, 0.75\%$ and 0.8%, two at each $\Delta\varepsilon$ level. Figure 9.a and 9.b show symmetric $\Delta\sigma\Delta\varepsilon$ loops measured in standard push-pull εN specimens under two fixed $\Delta\varepsilon$ ranges, which indicate cyclic hardening and loop stabilization. Figure 10.a illustrates the strain loops fitted to find the Al alloy cyclic Ramberg-Osgood coefficient and exponent H_c e h_c, listed in Tab. 3. Figure 10.b shows the obtained εN curve, with Coffin-Manson's rule fitting particularly well the experimental data of the 6351-T6 Al alloy tested in this work. The Coffin-Manson properties of this Al alloy are listed in Tab. 4.

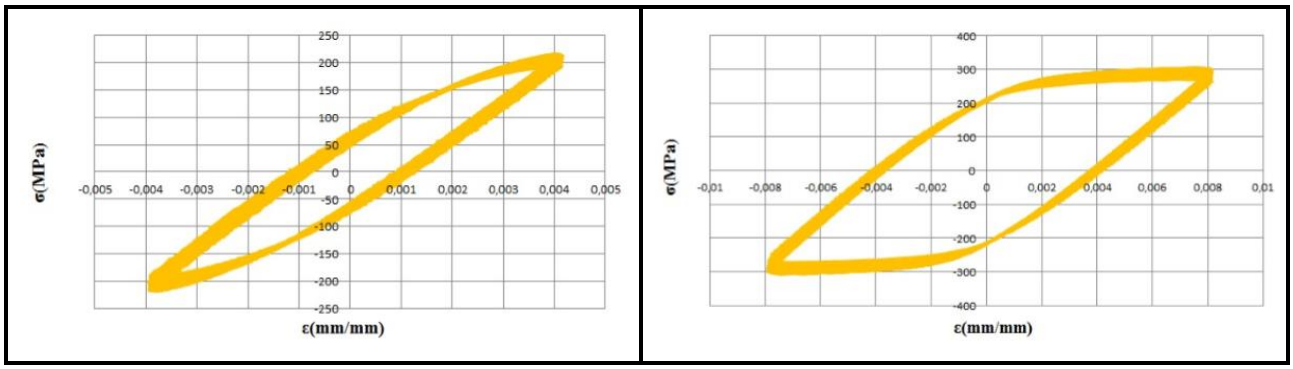

(a) (b)

Figure 9 – Stabilized push-pull loops measured in standard εN test specimens: (a) Δε = 0.4%; (b) Δε = 0.8%.

Table 3 – Ramberg-Osgood Cyclic properties

H_c (MPa)	h_c
717.18	0.152

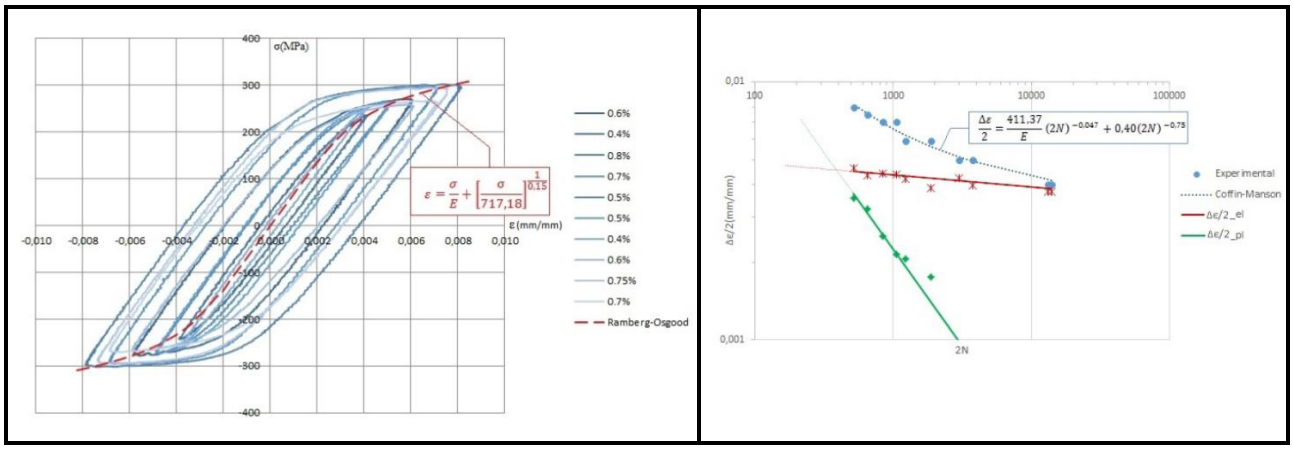

(a) (b)

Figure 10 – (a) Variable $\Delta\sigma\Delta\varepsilon$ loops in εN test specimens; (b) Coffin-Manson curve fitted to data measured by testing 6351-T6 Al alloy εN test specimens

Table 4 – Coffin-Manson properties

σ_c (MPa)	ε_c	b	c
411.36	0.4	-0.047	-0.75

Since stresses and strains should be purely elastic at "infinite lives", it is possible to estimate the fatigue limit from the elastic part of Coffin-Manson and Hooke equations. Thus, Eq. (5) does not need to use the Ramberg-Osgood cyclic properties, eliminating a possible source of error. Assuming the infinite life for Al alloy at $N_L = 5{\cdot}10^8$ cycles, using the measured Young's modulus $E = 68.2$GPa and Tab. 4 properties, this life corresponds to $\Delta\sigma = 311$ MPa, so to the stress amplitude $\sigma_a = 155.5$ MPa.

$$\left(\frac{\Delta\sigma}{E}\right) = 2\left(\frac{411.36}{E}\right)(2N_L)^{-0.047} \tag{5}$$

Using empirical fatigue strength modifying factors, Mischke proposed for polished surfaces, $k_{sf} = 1$; Juvinall's recommendation for diameters smaller than 8 mm, $k_{sz} = 1$, for alternated bending loads, $k_{ld} = 1$ and for pure axial loads $k_{ld} = 0.9$; as there is no abrupt change in temperature, the initial temperature is assumed as a parameter to determine k_Θ.

$$k_\Theta = 0.988 + 6.52 \cdot 10^{-4}\Theta - 3.42 \cdot 10^{-6}\Theta^2 + 5.63 \cdot 10^{-9}\Theta^3 - 6.25 \cdot 10^{-12}\Theta^4 \tag{6}$$

Where Θ is the working temperature, so, $k_\Theta \approx 1.002$. As the values of this empirical fatigue strength modifying factor is small, the approximation kQ = 1 is used here. So, with these factors estimated and replaced in Eq. (2), it is possible to compare in Tab. 5 the fatigue limit estimate recommended by Juvinall for this 6351 Al alloy (based on its ultimate tensile strength only) with the thermographic and the εN-based measurements presented in this work.

Table 5 – Estimates for fatigue limit of the Al 6351 Al alloy

S_U-based (MPa)	Risitano (MPa)	εN extrapolation (MPa)
130	168	155.38

CONCLUSIONS

This work reports a study about the problems found when using the thermographic methodology for the rapid determination of the fatigue limit of an Al 6351 T6 alloy, and the verification of the results obtained by extrapolating its εN curve measured by standard procedures to a life of $5{\cdot}10^8$ cycles. It is important to note that thermographic approach significantly reduces the fatigue testing costs by much reducing the testing time and the quantity of specimens required.

However, the number of cycles of first thermal phase of the tested Al alloy depends on the stress amplitude, unlike what happens for steels. The difficult in stabilizing the test specimen temperature during the thermographic tests can be associated the high thermal conductivity of the Al alloys, which rapidly dissipates the heat generated by the cyclic plastic deformations observed above the fatigue limit. The estimated value of the fatigue limit obtained by thermography is 168 MPa, and by extrapolation of the εN data is 155MPa, approximately eight percent smaller. Both are much higher than the classical 130MPa estimation proposed by Juvinall in the absence of proper experimental data, indicating that, as expected, his estimate can be too conservative. Finally, it is important to emphasize that as the actual measurements of fatigue limits for Al alloys by the Dixon or the Prot methods is an impossible task in most practical applications, both the thermography and the εN extrapolation can be viable options for the unreliable estimates proposed in the literature.

REFERENCES

ASTM E466, 2015. “Standard practice for conducting force controlled constant amplitude axial fatigue tests of metallic materials.” Chapter 5.

ASTM E606, 2012 “Standard test method for strain-controlled fatigue testing”.

Bandeira, C.F.B., Kenedi, P.P. and Castro, J.T.P, 2018, “On the use of thermographic method to measure fatigue limits”, Latin American Journal of Solids and Structures, 2018, 15(10 Thematic Section), e60.

Bandeira, C.F.B., Kenedi, P.P. and Castro, J.T.P, 2017, “Thermography – a faster method to obtain the fatigue or endurance limit of materials”, International Symposium on Solid Mechanics, 6th Edition.

Bandeira C. F. C., Kenedi P. P.; Castro J. T. P., Meggiolaro M. A., 2017. “On the use of the thermographic technique to determine the fatigue limit of a cold drawn carbon steel”. Seventh International Conference on Very High Cycle Fatigue, p. 329-334, U. Siegen. ISBN 978-3-00-056960-9.

Boyer, Howard E., 1985. “Atlas of Fatigue Curves.” ASM International.

Castro J. T. P., Meggiolaro M. A., 2016. “Fatigue Design Techniques, volume 1: High-Cycle Fatigue.” CreateSpace.

Castro J. T. P., Meggiolaro M. A., 2016. “Fatigue Design Techniques, volume 2: Low-Cycle and Multiaxial Fatigue.” CreateSpace.

Dixon,WJ. The up-and-down method for small samples. Am Stat Assoc J 60(312):967-978, 1965

Dowling E. Norman, “Mechanical behavior of materials: engineering methods for deformation, fracture, and fatigue.” Pearson

Fargione G., Gerarci A., La Rosa G., Risitano, 2002. A rapid determination of the fatigue curve by the thermographic method. International Journal of Fatigue, Vol. 24, p. 11-19.

Guamán A., Castro J. T. P., Vieira R. B., Paiva V. E. L., Freire J. L. F., 2017. “Fatigue Limit Assessment of a Low Carbon Steel using Dixon’s Up-And-Down and Infrared Thermography Methods” International Conference on Advances in Experimental Mechanics 29th – 31st August 2017, University of Sheffield, UK.

Haibach, E “Modified linear damage accumulation hypothesis accounting for a decreasing fatigue strength during increasing fatigue damage”, LBF TM Nr.50, Darmstadt, Germany, 1970.

Juvinall, RC. Stress, Strain & Strength, McGraw-Hill 1967.

La Rosa G, Risitano A., 1999. Thermographic methodology for the rapid determination of the fatigue limit of materials and mechanical components. In J Fatigue Mater Struct Components 1999; Vol 22, p. 65-73.

Prot, E. Marcel, “Fatigue testing under progressive loading, a new technique for testing materials”, Revue de Metallurgie, Vol. XLV No.12, 1948, p. 481.

Shigley, JE; Mischke, CR; Budynas, RG. Mechanical Engineering Design, 7th ed. McGraw-Hill 2004.

RESPONSIBILITY NOTICE

The authors are the only responsible for the printed material included in this paper.